NANO LETTERS

Letter

pubs.acs.org/NanoLett

Vibrational Mismatch of Metal Leads Controls Thermal Conductance of Self-Assembled Monolayer Junctions

Shubhaditya Majumdar,[†] Jonatan A. Sierra-Suarez,[‡] Scott N. Schiffres,[†] Wee-Liat Ong,[†] C. Fred Higgs, III,[†,‡] Alan J. H. McGaughey,[†,§] and Jonathan A. Malen*[,†,§]

[†]Department of Mechanical Engineering, [‡]Department of Electrical and Computer Engineering, and [§]Department of Materials Science and Engineering, Carnegie Mellon University, 5000 Forbes Avenue, Pittsburgh 15213, United States

Supporting Information

ABSTRACT: We present measurements of the thermal conductance of self-assembled monolayer (SAM) junctions formed between metal leads (Au, Ag, Pt, and Pd) with mismatched phonon spectra. The thermal conductance obtained from frequency domain thermoreflectance experiments is 65 ± 7 MW/m^2 K for matched Au−alkanedithiol−Au junctions, while the mismatched Au−alkanedithiol−Pd junctions yield a thermal conductance of 36 ± 3 MW/m^2 K. The experimental observation that junction thermal conductance (per molecule) decreases as the mismatch between the lead vibrational spectra increases, paired with results from molecular dynamics (MD) simulations, suggest that phonons scatter elastically at the metal−SAM interfaces. Furthermore, we resolve a known discrepancy between measurements and MD predictions of SAM thermal conductance by using a contact mechanics model to predict 54 ± 15% areal contact in the Au−alkanedithiol−Au experimental junction. This incomplete contact obscures the actual junction thermal conductance of 115 ± 22 MW/m^2 K, which is comparable to that of metal−dielectric interfaces.

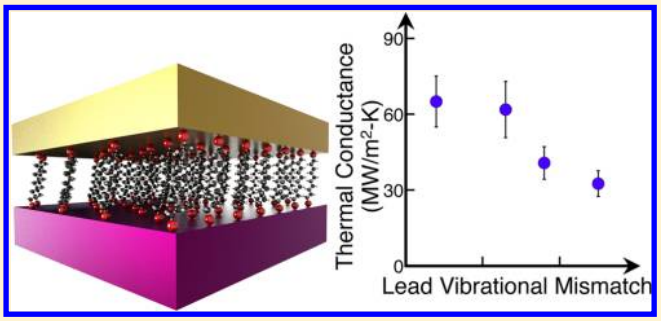

KEYWORDS: *Nanoscale, molecular junctions, thermal transport, self-assembly, thermoreflectance, molecular dynamics*

Hybrid materials exploit intimate structured connections between organic and inorganic components to create unique energy and charge transport landscapes, showing promise for application in electronics,[1−6] light-emitting diodes,[7,8] solar cells,[9−11] and thermoelectrics.[12−19] The lifetime and efficiency of such micro- or nanoscale devices is affected by their operating temperature so that it is critical to know their thermal properties.[20,21] For hybrid materials, the thermal conductance of the internal organic−inorganic interfaces plays a key role.[22−24] Our focus here is on self-assembled monolayers[25−30] (SAMs), two-dimensional periodic arrays of organic molecules that form spontaneously from solution on metal or dielectric surfaces. A SAM junction is formed when the SAM is sandwiched between two leads, as shown in Figure 1a. SAM junctions are a unique platform for studying thermal and electronic transport across a single molecular layer, where discrete vibrational and electronic states in the molecules bridge continuous energy bands in the inorganic leads. For the alkane-based SAMs investigated here, vibrations dominate thermal transport across the junctions since electronic transport is only possible through weak off-resonant tunneling mechanisms.[14,15,31−34]

Early measurements suggested that SAM junction thermal conductance is limited by the molecule−lead interfaces. Wang et al.[22] probed thermal transport through an alkanethiol SAM grown on Au. They found that the major thermal resistance was the Au−SAM interface (thermal conductance of 220 ± 100 MW/m^2 K) and that thermal transport within the molecules was ballistic. Wang et al.[26] studied metal−SAM−semiconductor (Au−alkanedithiol−GaAs) junctions and reported a junction thermal conductance of 28 ± 3 MW/m^2 K that did not vary with molecular length (8−10 CH_2 groups), corroborating ballistic thermal transport within the molecules. Meier et al.[29] also reported a length-invariant thermal conductance for alkanethiol SAMs having more than 10 carbon atoms but found an increasing thermal conductance with shortening of the chain length.

The strength of the interfacial bonding between the molecule headgroup and the lead has also been found to affect thermal transport across SAM junctions. Using Au−SAM−SiO_2 junctions with alkane-based SAMs, Losego et al.[27] showed that higher interfacial bonding strength can increase the junction thermal conductance from 30 to 65 MW/m^2 K. O'Brien et al.[28] found that SAMs could be used to increase the interface thermal conductance between a metal and a dielectric by increasing the interfacial adhesion energy as well as augmenting the overlap region of the molecule and lead vibrational states. The effect of adhesion energy has also been

Received: December 17, 2014
Revised: March 4, 2015
Published: April 17, 2015

DOI: 10.1021/nl504844d
Nano Lett. 2015, 15, 2985−2991

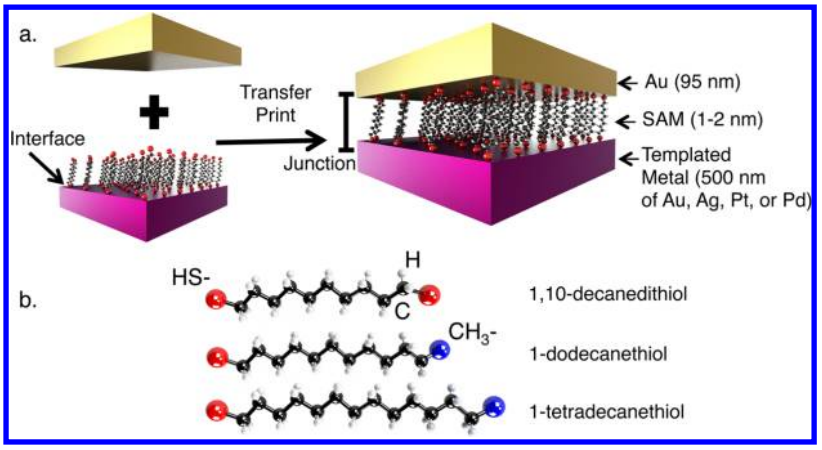

Figure 1. (a) Schematic diagram of the transfer printing process to create a SAM junction. A 95 ± 5 nm Au layer is transfer printed onto a SAM grown on a 475−530 ± 20−30 nm (see Supporting Information Table S4) templated metal substrate. (b) Straight chain alkane-based molecules are used to create the SAMs in this study (1,10-decanedithiol, 1-dodecanethiol, and 1-tetradecanethiol).

investigated for Au−liquid and Au−SAM−liquid systems, where higher wettability of the liquid on the SAM due to higher adhesion energy led to increased interface thermal conductance.[35,36]

Computational efforts to quantify thermal transport in organic−inorganic systems have led to similar conclusions. Segal et al.[37] predicted that for junctions comprised of alkane chains with more than 10 carbon atoms in contact with 2 leads, inelastic effects at the interfaces and within the molecules are insignificant. They found the thermal conductance of the junction to be independent of molecular length in this range at a temperature of 300 K, consistent with experimental measurements.[26,29] Predictions from molecular dynamics (MD) simulations have found interface thermal conductance to increase with increasing interfacial bond strength and increasing vibrational overlap between molecule and substrate.[28,30,38−40] The predicted values of junction thermal conductance from MD simulations,[38−40] however, are at least a factor of 2 higher than those measured in experiments.[26−28,30] Resolution of this discrepancy is required to advance our understanding of phonon transmission at hybrid interfaces.

There has been no systematic investigation on the effect of the vibrational properties of the leads on thermal transport across SAM junctions. Experimental data are only available for metal−SAM−dielectric junctions,[26−28,30] wherein the vibrational properties of the two leads are highly mismatched. Using metals, it is possible to select leads with varying degrees of vibrational mismatch. In this Letter, we use thermoreflectance experiments and MD simulations of metal−SAM−metal junctions to investigate the effect of vibrational spectra overlap on the junction thermal conductance. We find that the thermal conductance (per molecule) is highest when the leads are the same and reduces as the vibrational mismatch increases. Furthermore, we reconcile the discrepancy between experimentally measured values of thermal conductance and those predicted from simulations by estimating the percentage contact area in the SAM junction using contact mechanics models[41] informed by atomic force microscopy (AFM) surface roughness data of our leads.

Metal−SAM−metal junctions were fabricated using a transfer printing technique[42] (Figure 1a). Molecules of 1,10-decanedithiol ($C_{10}H_{22}S_2$), 1-dodecanethiol ($C_{12}H_{26}S$), and 1-tetradecanethiol ($C_{14}H_{30}S$), as shown in Figure 1b, were used to grow the SAMs. Both dithiols and monothiols were considered to probe the effect of end-group chemistry. Metal films (Au, Ag, Pt, or Pd) of thickness 475−530 ± 20−30 nm (see Supporting Information Table S4) were fabricated through a templating technique.[43] The Au surface has a root-mean-square (RMS) roughness of 4 ± 1 Å measured using AFM, consistent with prior Au templates.[43,44] These samples were then immersed in a dilute solution (0.1 mM) of the SAM molecules in ethanol for 18−24 h.[25,45] A 95 ± 5 nm Au film (originally evaporated onto a Si wafer, then lifted off using a PDMS stamp) was then transfer printed onto these structures to complete the junction (see Supporting Information S1.1 and S2). Transfer printing the top film prevents damage to the SAM, as has been observed when a high-energy deposition process such as sputtering or evaporation is used to create the junction.[42,46,47] Thus, the junctions have the configuration metal−SAM−Au, where the bottom metal lead is Au, Ag, Pt, or Pd, the top lead is Au, and the SAM is an alkanedithiol or alkanethiol. At least five samples were made of each configuration.

The metal−SAM interface was characterized through X-ray photoelectron spectroscopy (XPS) measurements (S1.2) to study the atomic composition and bonding environment. The measurements confirmed the presence of the SAM and the absence of a parasitic oxide layer that could affect SAM coverage and add thermal resistance. Ellipsometry measurements were also performed to measure the SAM thickness and were found to agree with previous studies (S1.3).[25,48]

The SAM junction thermal conductance was measured at an ambient temperature of 296 K using frequency domain thermoreflectance (FDTR), a noncontact laser-based measurement technique.[23,49] An intensity modulated pump laser (488 nm) periodically heats the sample surface (the topmost 95 nm Au film), leading to a periodic surface temperature oscillation. This temperature oscillation is probed using a second laser (532 nm) based on the high thermoreflectance of the topmost Au lead. An analytical solution to the heat diffusion equation for a semi-infinite layered system heated by a Gaussian-shaped periodic surface heat flux is fit to the phase lag of the sample surface temperature with respect to the applied heat flux.[23,50] Representative phase lags for Au−alkanedithiol−Au and Au−alkanethiol−Au SAMs are plotted in Figure 2a versus modulation frequency. The solid lines correspond to the solution of the heat diffusion equation with junction thermal conductance as the only fitting parameter. There is a stark

DOI: 10.1021/nl504844d
Nano Lett. 2015, 15, 2985−2991

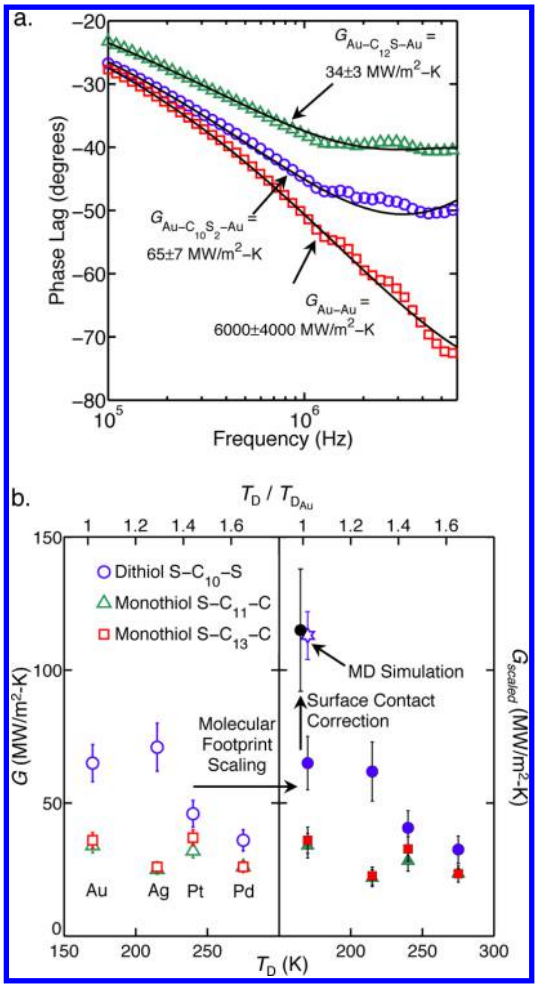

Figure 2. (a) FDTR phase responses for junctions with 1,10-decanedithiol, 1-dodecanedithiol, and no molecules are clearly distinguishable. Solid lines represent the best-fit solutions of the heat diffusion equation for a semi-infinite layered system heated by a Gaussian-shaped periodic heat flux at the surface. (b) Variation of junction thermal conductance G with the Debye temperature of the templated metal substrate on which the SAM is grown. The raw experimental data (left panel, unfilled data points) are scaled by the molecular footprint (right panel, filled data points) to isolate the effect of the leads vibrational spectra on G. Also plotted is the MD prediction of G for a Au–(1,10-decanedithiol)–Au junction (unfilled star) and the percentage area corrected experimental thermal conductance (filled black circle), which has been displaced slightly to the left for clarity. All experiments were performed at an ambient temperature of 296 K.

difference in the phase responses between these two configurations with junction thermal conductances of 65 ± 7 and 34 ± 3 MW/m^2 K. They also differ from the phase response of a Au–Au interface (no SAM), also plotted in Figure 2a. These phase responses demonstrate the sensitivity of our measurements to the possibility of metal–metal shorting across the SAMs and indicate that such shorting is not present. Supporting this conclusion, previous studies of SAM junctions created through transfer prints have shown a high degree of repeatability in creating junctions without shorting between the electrodes.[51,52] Measurements were made for at least five different laser spot locations on each sample. These results demonstrate the sensitivity of the phase response in FDTR to the presence and chemistry of the SAM.

The measured junction thermal conductances for all configurations are plotted in the left panel of Figure 2b versus the Debye temperature (T_D) of the metal contact on which the SAM is grown (for a list of Debye temperatures, see Supporting Information S3). The uncertainty of an individual thermal conductance measurement (as reported in Figure 2a) was calculated from the fitted thermal model by accounting for the uncertainty in the properties of the layered sample.[23,49] The error bars in Figure 2b represent the combination of the uncertainties of the individual measurements with the variability arising from different spot locations and samples using a statistical model, details of which are provided in Supporting Information S4. The Debye temperature is an estimation of the temperature at which all vibrational states in a system are activated. It can thus be used to characterize the extent of the vibrational frequency spectrum for a material.[37,53,54] We use the Debye temperature as a measure of the vibrational mismatch between the two metal leads (Au with either Au, Ag, Pt, or Pd) in a particular SAM junction. Au has the lowest Debye temperature ($T_{D_{Au}}$ = 170 K) and thus Debye temperature mismatch between the leads increases (i.e., the ratio $T_D/T_{D_{Au}}$ increases) as we move from left to right along the horizontal axis in both panels of Figure 2b.

The 1,10-decanedithiol SAMs exhibit a larger range of junction thermal conductances (mean values of 36 to 71 MW/m^2 K) than either the 1-dodecanethiol or 1-tetradecanethiol SAMs (25 to 37 MW/m^2 K). The two monothiols have comparable junction thermal conductance values for all configurations, corroborating the previously reported length independence for alkane chains having more than 10 carbon atoms.[26,29,37,53] Our measurements are comparable to previous measurements of junction thermal conductance of Au–1,10-decanedithiol–GaAs[26] (28 ± 3 MW/m^2 K) and Au–(11-mercapto-undecyltrimethoxysilane)–quartz[27] (65 ± 5 MW/m^2 K) junctions. As further confirmation, we also fabricated Au–decanedithiol–GaAs junctions and measured a thermal conductance of 32 ± 4 MW/m^2 K, which is in agreement with the result of Wang et al.[26]

The junction thermal conductance plotted in the left panel of Figure 2b is related to the molecular footprint (i.e., the projected area per molecule) of the SAM, which depends on the lead on which it is grown.[25,48,55] To isolate the effect of the vibrational properties of the leads from the footprint effect, we scaled the measured experimental data (G) using the molecular footprint of the 1,10-decanedithiol SAM (σ_{SAM-Au}) grown on Au according to

$$G_{scaled} = \frac{\sigma_{SAM-metal}}{\sigma_{SAM-Au}} G \quad (1)$$

Here, $\sigma_{SAM-metal}$ is the molecular footprint (Supporting Information S5) of the SAM on the bottom metal lead (Au, Ag, Pt, or Pd). The scaled data (G_{scaled}) is plotted in the right panel of Figure 2b. The scaled junction thermal conductance decreases as the difference in the Debye temperatures of the leads increases. The reduction is strong for the 1,10-decanedithiol SAMs and weak for the 1-dodecanethiol and 1-tetradecanethiol SAMs. The values of $\sigma_{SAM-metal}$ for the systems investigated here are within 15% of each other, a range comparable to the error bars associated with the thermal conductance measurements plotted in Figure 2b. The total range of thermal conductances of the Au–alkanedithiol–metal systems is larger than this uncertainty, giving us confidence in

DOI: 10.1021/nl504844d
Nano Lett. 2015, 15, 2985–2991

the observed decreasing trend. We hypothesize that the decrease happens as the combined overlap between the density of states (DOS) of the leads and the discrete vibrational states of the molecules decreases, or equivalently as the Debye temperatures of the leads diverge. The weak trend for the monothiol SAMs is likely due to the weak metal−CH_3 bond acting as the dominant resistance to thermal transport, thus overpowering the effect of the mismatched metal leads.

Though in agreement with similar measurements,[26−30] our thermal conductance for the Au−alkanedithiol−Au junction (65 ± 7 MW/m^2 K) is a factor of 2 lower than our MD prediction (113 ± 9 MW/m^2 K, plotted as a white star in the right panel of Figure 2b, discussed later) and the MD prediction (200 ± 60 MW/m^2 K) by Luo and Lloyd.[40,56] We hypothesize that a major source of this discrepancy is that the surface roughness of the Au leads causes imperfect surface contact within the junction. To test this hypothesis, we calculated the percentage contact between the leads upon transfer printing using a rough surface contact model.[41] The model is an extension to the work of Kogut and Etsion[57] (the KE model), who included finite element analysis (FEA)-validated plasticity effects while determining surface deformations. The rough surface is modeled as a collection of spherical asperity tips with areal density and dimensions based on surface topography data obtained using AFM (shown in Figure 3a). The contact between the two rough surfaces is made mathematically equivalent to a single rough surface in contact with a smooth one, as illustrated in Figure 3b, and originally proposed by Greenwood and Tripp.[58] The balance between the reaction pressure and attractive adhesive pressure allows us to predict the contact area of the asperities.

Previous studies that predicted percentage contact area only considered adhesion stemming from van der Waals bonding at the surface characterized by a Lennard-Jones (LJ) potential.[59−61] The strong thiol−Au interaction[62,63] in our system required us to modify the adhesion force calculation derived by Derjaguin et al.[59] and Muller et al.[60] (the DMT model) by using a Morse potential instead of the LJ potential.[41] Furthermore, previous applications of the DMT model considered asperities comprised of one material. In our case, we have a SAM grown on Au, which creates a composite asperity, as shown in Figure 3c. To account for the SAM, the total adhesion force between the asperity and the flat surface was assumed to be a linear combination of adhesion forces for each shell. Our contact model, like the DMT and KE models, is based on the assumptions originally made by Greenwood and Tripp:[58] (i) the analysis is valid for a surface profile that is isotropic with a Gaussian distribution of peak heights, (ii) a single asperity tip is not influenced by the deformation of neighboring asperities, and (iii) the bulk solid behind the asperity layer is rigid. In addition, we also assumed that the SAM layer has the same elastic properties as the deforming metal asperity it is grown on.

From our analysis, we predict the percentage contact area A^* for the Au−alkanedithiol−Au junction to be 54 ± 15%. The measured junction thermal conductance can be related to A^* and that of a perfect contact through the analysis described by Seong et al.[64] and Prasher et al.[65] Together with the experimental measurement of 65 ± 7 MW/m^2 K for the Au−alkanedithiol−Au junction, we thus predict a perfect contact junction thermal conductance of 115 ± 22 MW/m^2 K, which is plotted as a black circle in the right panel of Figure 2b. This value agrees with our MD prediction and supports our

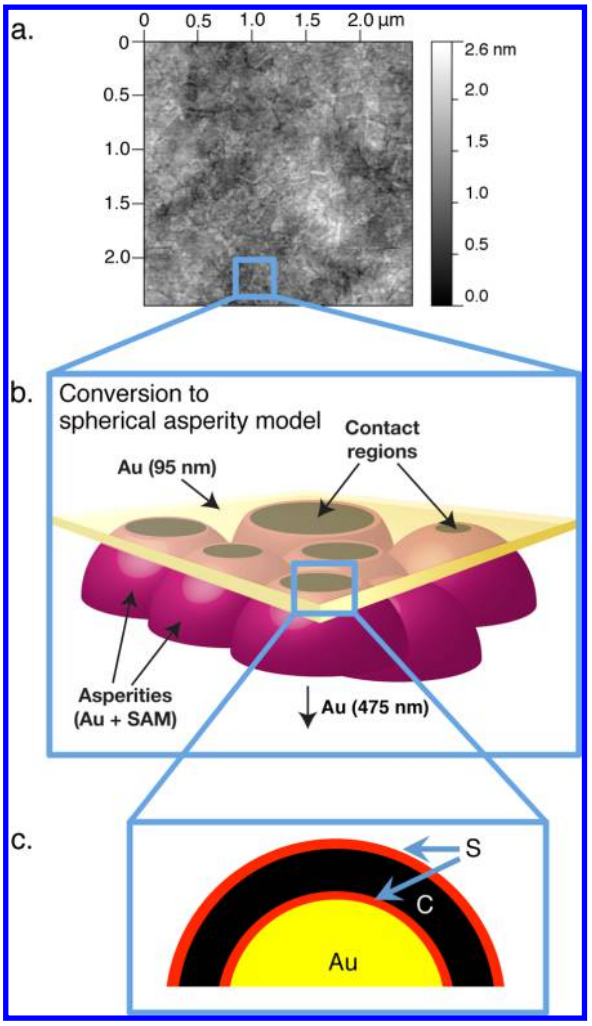

Figure 3. (a) AFM image of a templated Au lead (RMS roughness 4 ± 1 Å). (b) Schematic diagram of two rough surfaces represented as spherical asperities (475 nm Au + SAM) in contact with a flat, undeformable surface (95 nm Au). (c) A single asperity is a layered, composite structure consisting of an outer shell of the SAM molecules [S (red) and C (black) atoms] enclosing an inner Au core. Interactions between all atoms and the upper Au surface are considered when calculating the percentage contact area.

hypothesis that the source of the discrepancy between experimental measurements and MD simulations is incomplete contact. Although measured RMS roughnesses of templated Ag, Pd, and Pt samples are similar to that of Au,[43] new interatomic potentials for the thiol−metal bonds would be required to apply our contact mechanics model to those junctions. As such, we cannot rigorously confirm the universality of this result.

To further probe the vibrational coupling effects in the SAM junctions presented in Figure 2b, we performed MD simulations using LAMMPS[66] of Au−alkanedithiol−Au structures representative of the experimental setup (Supporting Information S6). Our MD simulation structure has a cross-sectional area of 2.5 × 2.5 nm^2 and represents a region of perfect contact. To mimic the experiments, the SAM was first created on a Au substrate. This system was relaxed in a canonical ensemble at a temperature of 300 K resulting in a steady-state tilt angle of 26 ± 5°, which agrees with experimental observations of 30 ± 7°.[25] The second substrate was then placed on the SAM (similar to the transfer print step)

DOI: 10.1021/nl504844d
Nano Lett. 2015, 15, 2985−2991

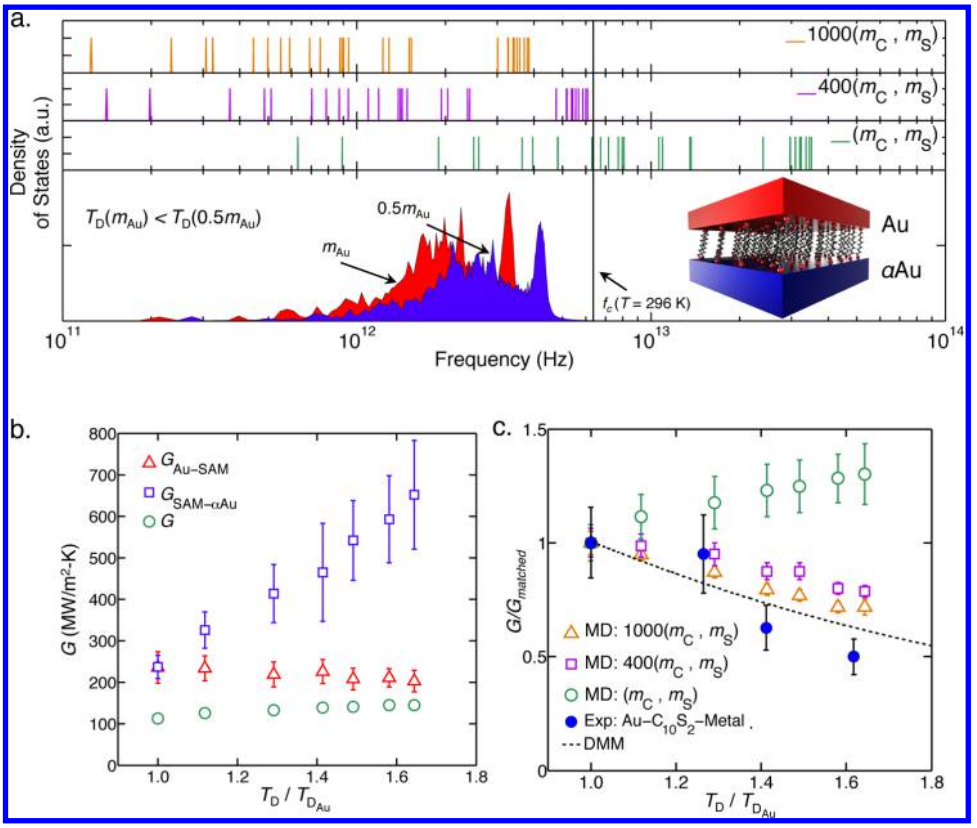

Figure 4. (a) DOS of the metal leads with atomic masses m_{Au} (red) and $0.5m_{Au}$ (blue), and 1,10-decanedithiol having carbon and sulfur atoms with atomic masses (m_C,m_S) (green), ($400m_C$,$400m_S$) (purple), and ($1000m_C$,$1000m_S$) (orange). (b) MD-predicted variation of the thermal conductance of the individual interfaces (blue square and red triangles) and the entire junction (green circles) with the Debye temperature ratio of the metal leads. (c) Variation of junction thermal conductance, normalized by the value of the matched lead case, with the Debye temperature ratio of the metal leads. The MD predictions (orange triangles, purple squares, and green circles) are compared to the experimental results (blue filled circles) and DMM calculations (dashed line).

and the entire system was relaxed again at a temperature of 300 K. Nonequilibrium molecular dynamics was employed to predict a temperature difference across the junction for a known heat flux q''. The junction thermal conductance was calculated using $G = q''/\Delta T$, where ΔT is the temperature drop across the entire junction.

To model the effect of mismatched metal leads, we varied the atomic mass (m) of one lead. We assume that the main contribution to the vibrational properties is from the atomic mass of the lead. This approximation is reasonable because all of the metals in our experiments are face-centered cubic with similar lattice constants. If the ratio of the bottom lead atomic mass with respect to that of Au is $\alpha = m/m_{Au}$, its Debye temperature (T_D) can be set from

$$\frac{T_D}{T_{D_{Au}}} = \alpha^{-1/2} \tag{2}$$

Vibrational DOS calculations were performed using velocity autocorrelation data from MD simulations for the bulk leads and lattice dynamics calculations using GULP[67] for the molecules (Supporting Information S7). The predicted DOS for two leads whose atoms have masses of m_{Au} and $0.5m_{Au}$ (comparable to the atomic mass of Pd) are plotted in the bottom panel of Figure 4a. The discrete states of 1,10-decanedithiol molecule are plotted in the panel immediately above the lead DOS (in green).

The junction thermal conductance of such mismatched systems depends strongly on the nature of vibrational scattering at the individual metal−SAM interfaces. For an elastic scattering event, the frequencies of the reflected and/or transmitted energy carriers are the same as that of the incident energy carrier. For an inelastic (i.e., anharmonic) event, the scattered frequencies will be different. If only elastic scattering is present at the interfaces and the thermal transport in the SAM is ballistic, the metal lead having the DOS with the narrowest spectrum will dictate the highest frequency that can transmit energy across the entire junction and contribute to the junction thermal conductance. Vibrational modes with frequencies above this cutoff will be fully reflected from the interface. This scenario would imply that as the vibrational spectra of the two leads increase in mismatch, the junction thermal conductance would decrease because the number of overlapping vibrational modes between the SAM and the two leads would also decrease. This hypothesis is consistent with our experimental measurements, suggesting the dominance of elastic scattering at the interfaces.

The variation of the junction thermal conductance with the lead Debye temperature ratio ($T_D/T_{D_{Au}}$) from MD simulations is plotted in Figure 4b (green circles). In contrast to our experimental measurements, the junction thermal conductance increases by a factor of 1.3 as $T_D/T_{D_{Au}}$ increases. We also plot the metal−SAM interface thermal conductances on either side of the junction in Figure 4b. The thermal conductance of the interface whose Debye temperature is varied ($G_{SAM-\alpha Au}$) increases as the Debye temperature increases, while the

DOI: 10.1021/nl504844d
Nano Lett. 2015, 15, 2985−2991

interface conductance at the Au lead (G_{Au-SAM}) remains constant. These observations contradict our experimental measurements and suggest that overlap between the vibrational states at each interface in the MD simulations is independently realized.

Why do the interfaces in our MD simulations act independently while those in the experiments appear not to? Noting that MD simulations obey classical (i.e., Boltzmann) statistics, all vibrational states are activated. From Figure 4a, we see that many vibrational states in the molecule have frequencies higher than the characteristic thermal frequency $f_c = k_B T/h$ (where k_B is the Boltzmann constant and h is the Planck constant), which is 6.2 THz at a temperature of 296 K. While active in the MD simulations, these modes are frozen out in the experiments. Furthermore, the maximum frequency for the lightest lead (Pd, T_D = 275 K) lies below this cutoff such that all the lead states are fully active for all the experimental systems.

We hypothesize that the classical nature of the MD simulations and inelastic scattering effects within the molecules themselves lead to predictions different from the experimental measurements. The atomic interactions in our MD simulations are anharmonic, which allows inelastic processes to occur within the molecules. Because all of the vibrational states are active in the MD simulations, an anharmonic scattering event within the SAM involving three vibrational states could facilitate down-conversion of modes above the frequency cutoff of the heavier lead. In particular, one mode above the cutoff can scatter into two modes below the cutoff, creating additional channels for vibrational coupling across the junction. Such events cannot occur in the experiments because vibrational modes with characteristic temperatures above 296 K are not activated. Anharmonic events within the SAM would allow each metal lead to interact with the SAM independently, as seen in the MD results, therein opening pathways for thermal transport across the junction that are not present in the experiments.

To test this hypothesis, the vibrational spectrum of the SAM needs to be restricted to coincide with the activated spectrum in the experiments. As the classical nature of MD forces all available vibrational states to be activated, the states themselves need to be changed. To lower the molecular frequencies, the mass of the carbon and sulfur atoms are increased to 400 and 1000 times their actual values. The DOS for these modified molecules are plotted in the top panels of Figure 4a (purple and orange). The junction thermal conductance of the modified configurations is plotted in Figure 4c (purple squares and orange triangles) along with the original MD results and the molecular footprint-scaled experimental data (G_{scaled}). The data is normalized with respect to the junction thermal conductance of the matched lead case ($G_{matched}$) of each set. As the SAM molecules get heavier and their frequency spectrum is reduced, $G/G_{matched}$ decreases with increasing $T_D/T_{D_{Au}}$ in agreement with our experimental trend.

We also derived a modified form of the diffuse mismatch model (DMM) model used by Duda et al.,[53] wherein the vibrational modes participating in thermal transport through the junction are limited by the lead with the narrowest DOS (Supporting Information S8). The prediction of $G/G_{matched}$ using this model is plotted as a dashed line in Figure 4c and agrees with our experimental and modified MD trends. These findings support our hypothesis that elastic scattering mechanisms dominate within the SAM junctions and at each metal−SAM interface in the experiments, therein explaining why vibrational mismatch of the leads reduces G.

In summary, we experimentally probed how the selection of leads affects the thermal conductance of metal−SAM−metal junctions. We found the junction thermal conductance to decrease as the vibrational mismatch increases. The discrepancy between the experimental measurement of the Au−alkanedithiol−Au junction thermal conductance and that predicted from MD simulations was resolved by correcting for the true contact area realized in the experiments using a contact mechanics model for rough surfaces. We thus see that thermal transport properties of SAM junctions can be manipulated by adjusting lead material as well as end-group chemistry.

■ ASSOCIATED CONTENT

Supporting Information

More detailed information on templating, transfer printing, XPS and ellipsometry measurements, FDTR measurement and uncertainty analysis, MD simulations, DOS calculations, and the Landauer formalism to calculate interface thermal conductance using the DMM. This material is available free of charge via the Internet at http://pubs.acs.org.

■ AUTHOR INFORMATION

Corresponding Author

*E-mail: jonmalen@andrew.cmu.edu.

Author Contributions

S.M. synthesized the SAM junctions, conducted the FDTR experiments, assisted in the contact mechanics analysis, and performed the MD simulations and the LD calculations. J.A.S−S. performed the contact mechanics analysis and the AFM measurements. S.N.S. assisted in sample synthesis and FDTR measurements. W-L.O. assisted with the FDTR measurements and the MD simulations. S.M. wrote the paper. J.A.S−S., S.N.S., W-L.O., C.F.H., A.J.H.M., and J.A.M. edited the paper. All authors discussed the data and commented on the results in the paper.

Notes

The authors declare no competing financial interest.

■ ACKNOWLEDGMENTS

We acknowledge Mark Losego (Georgia Tech) for his guidance in performing the transfer prints. At Carnegie Mellon University, we thank Matthew Payne and Chunrong Yin for performing the XPS measurements, John Riley for performing the ellipsometry measurements, Jason Wolf for performing the XRR measurements, and Adam Wise for assisting with the AFM measurements. We acknowledge support from the National Science Foundation (NSF) CAREER Award (Award No. ENG-1149374), the NSF Award (Award No. CCF-0811770), and the American Chemical Society (ACS) PRF DNI Award (Award No. PRF51423DN10).

■ REFERENCES

(1) Xu, B.; Tao, N. J. *Science* **2003**, *301*, 1221−1223.
(2) Joachim, C.; Gimzewski, J. K.; Aviram, A. *Nature* **2000**, *408*, 541−548.
(3) Nitzan, A.; Ratner, M. A. *Science* **2003**, *300*, 1384−1389.
(4) Heath, J. R.; Ratner, M. A. *Phys. Today* **2003**, *56*, 43.
(5) Luo, Y.; Collier, P. C.; Jeppesen, J. O.; Nielsen, K. A.; Delonno, E.; Ho, G.; Perkins, J.; Tseng, H.-R.; Yamamoto, T.; Stoddart, J. F.; Heath, J. R. *ChemPhysChem* **2002**, *3*, 519−525.

DOI: 10.1021/nl504844d
Nano Lett. 2015, 15, 2985−2991

(6) Aswal, D. K.; Lenfant, S.; Guerin, D.; Yakhmi, J. V.; Vuillaume, D. *Anal. Chim. Acta* **2006**, *568*, 84−108.
(7) Colvin, V. L.; Schlamp, M. C.; Alivisatos, A. P. *Nature* **1994**, *370*, 354−357.
(8) Gather, M. C.; Köhnen, A.; Meerholz, K. *Adv. Mater.* **2011**, *23*, 233−248.
(9) Tang, J.; Kemp, K. W.; Hoogland, S.; Jeong, K. S.; Liu, H.; Levina, L.; Furukawa, M.; Wang, X.; Debnath, R.; Cha, D.; Chou, K. W.; Fischer, A.; Amassian, A.; Asbury, J. B.; Sargent, E. H. *Nat. Mater.* **2011**, *10*, 765−771.
(10) Ip, A. H.; Thon, S. M.; Hoogland, S.; Voznyy, O.; Zhitomirsky, D.; Debnath, R.; Levina, L.; Rollny, L. R.; Carey, G. H.; Fischer, A.; Kemp, K. W.; Kramer, I. J.; Ning, Z.; Labelle, A. J.; Chou, K. W.; Amassian, A.; Sargent, E. H. *Nat. Nanotechnol.* **2012**, *7*, 577−582.
(11) Weickert, J.; Dunbar, R. B.; Hesse, H. C.; Wiedemann, W.; Schmidt-Mende, L. *Adv. Mater.* **2011**, *23*, 1810−1828.
(12) Baheti, K.; Malen, J. A.; Doak, P.; Reddy, P.; Jang, S. Y.; Tilley, T. D.; Majumdar, A.; Segalman, R. A. *Nano Lett.* **2008**, *8*, 715−719.
(13) Malen, J. A.; Doak, P.; Baheti, K.; Tilley, T. D.; Majumdar, A.; Segalman, R. A. *Nano Lett.* **2009**, *9*, 3406−3412.
(14) Malen, J. A.; Doak, P.; Baheti, K.; Tilley, T. D.; Segalman, R. A.; Majumdar, A. *Nano Lett.* **2009**, *9*, 1164−1169.
(15) Jang, S. Y.; Reddy, P.; Majumdar, A.; Segalman, R. A. *Nano Lett.* **2006**, *6*, 2362−2367.
(16) Lee, W.; Reddy, P. *Nanotechnology* **2011**, *22*, 1−8.
(17) See, K. C.; Feser, J. P.; Chen, C. E.; Majumdar, A.; Urban, J. J.; Segalman, R. A. *Nano Lett.* **2010**, *10*, 4664−4667.
(18) Reiss, P.; Couderc, E.; De Girolamo, J.; Pron, A. *Nanoscale* **2011**, *3*, 446−489.
(19) Yee, S. K.; Malen, J. A.; Majumdar, A.; Segalman, R. A. *Nano Lett.* **2011**, *11*, 4089−4094.
(20) Garimella, S. V. *Microelectronics J.* **2006**, *37*, 1165−1185.
(21) Lee, W.; Kim, K.; Jeong, W.; Zotti, L. A.; Pauly, F.; Cuevas, J. C.; Reddy, P. *Nature* **2013**, *498*, 209−212.
(22) Wang, Z.; Carter, J. A.; Lagutchev, A.; Koh, Y. K.; Seong, N.-H.; Cahill, D. G.; Dlott, D. D. *Science* **2007**, *317*, 787−790.
(23) Ong, W.-L.; Rupich, S. M.; Talapin, D. V.; McGaughey, A. J. H.; Malen, J. A. *Nat. Mater.* **2013**, *12*, 410−415.
(24) Ong, W.-L.; Majumdar, S.; Malen, J. A.; McGaughey, A. J. H. *J. Phys. Chem. C* **2014**, *118*, 7288−7295.
(25) Love, J. C.; Estroff, L. A.; Kriebel, J. K.; Nuzzo, R. G.; Whitesides, G. M. *Chem. Rev.* **2005**, *105*, 1103−1169.
(26) Wang, R. Y.; Segalman, R. A.; Majumdar, A. *Appl. Phys. Lett.* **2006**, *89*, 1−4.
(27) Losego, M. D.; Grady, M. E.; Sottos, N. R.; Cahill, D. G.; Braun, P. V. *Nat. Mater.* **2012**, *11*, 502−506.
(28) O'Brien, P. J.; Shenogin, S.; Liu, J.; Chow, P. K.; Laurencin, D.; Mutin, P. H.; Yamaguchi, M.; Keblinski, P.; Ramanath, G. *Nat. Mater.* **2012**, *12*, 118−122.
(29) Meier, T.; Menges, F.; Nirmalraj, P.; Hölscher, H.; Riel, H.; Gotsmann, B. *Phys. Rev. Lett.* **2014**, *113*, 60801.
(30) Sun, F.; Zhang, T.; Jobbins, M. M.; Guo, Z.; Zhang, X.; Zheng, Z.; Tang, D.; Ptasinska, S.; Luo, T. *Adv. Mater.* **2014**, 1−7.
(31) Malen, J. A.; Yee, S. K.; Majumdar, A.; Segalman, R. A. *Chem. Phys. Lett.* **2010**, *491*, 109−122.
(32) Wold, D. J.; Haag, R.; Rampi, M. A.; Frisbie, C. D. *J. Phys. Chem. B* **2002**, *106*, 2813−2816.
(33) Engelkes, V. B.; Beebe, J. M.; Frisbie, C. D. *J. Am. Chem. Soc.* **2004**, *126*, 14287−14296.
(34) Venkataraman, L.; Klare, J. E.; Tam, I. W.; Nuckolls, C.; Hybertsen, M. S.; Steigerwald, M. L. *Nano Lett.* **2006**, *6*, 458−462.
(35) Ge, Z.; Cahill, D.; Braun, P. *Phys. Rev. Lett.* **2006**, *96*, 186101.
(36) Harikrishna, H.; Ducker, W. A.; Huxtable, S. T. *Appl. Phys. Lett.* **2013**, *102*, 251606.
(37) Segal, D.; Nitzan, A.; Hänggi, P. *J. Chem. Phys.* **2003**, *119*, 6840 1−16.
(38) Hu, L.; Zhang, L.; Hu, M.; Wang, J.-S.; Li, B.; Keblinski, P. *Phys. Rev. B* **2010**, *81*, 1−5.
(39) Luo, T.; Lloyd, J. R. *J. Appl. Phys.* **2011**, *109*, 034301.
(40) Luo, T.; Lloyd, J. R. *Int. J. Heat Mass Transfer* **2010**, *53*, 1−11.
(41) Sierra-Suarez, J. A.; Majumdar, S.; McGaughey, A. J. H.; Malen, J. A.; Higgs, C. F., III. Submitted for publication.
(42) Meitl, M. A.; Zhu, Z.-T.; Kumar, V.; Lee, K. J.; Feng, X.; Huang, Y. Y.; Adesida, I.; Nuzzo, R. G.; Rogers, J. A. *Nat. Mater.* **2006**, *5*, 33−38.
(43) Weiss, E. A.; Kaufman, G. K.; Kriebel, J. K.; Li, Z.; Schalek, R.; Whitesides, G. M. *Langmuir* **2007**, *23*, 9686−9694.
(44) Hegner, M.; Wagner, P.; Semenza, G. *Surf. Sci. Lett.* **1993**, *291*, 39−46.
(45) Bain, C. D.; Troghton, E. B.; Tao, Y.-T.; Whitesides, J. E. G. M.; Nuzzo, R. G. *J. Am. Chem. Soc.* **1989**, *111*, 321−335.
(46) Zhao, X.-M.; Xia, Y.; Whitesides, G. M. *J. Mater. Chem.* **1997**, *7*, 1069−1074.
(47) Kim, J. W.; Yang, K. Y.; Hong, S. H.; Lee, H. *Appl. Surf. Sci.* **2008**, *254*, 5607−5611.
(48) Laibinis, P.; Whitesides, G. *J. Am. Chem. Soc.* **1991**, *113*, 7152−7167.
(49) Malen, J. A.; Baheti, K.; Tong, T.; Zhao, Y.; Hudgings, J. A.; Majumdar, A. *J. Heat Transfer* **2011**, *133*, 081601.
(50) Cahill, D. G. *Rev. Sci. Instrum.* **2004**, *75*, 5119.
(51) Akkerman, H. B.; de Boer, B. *J. Phys.: Condens. Matter* **2008**, *20*, 013001.
(52) Loo, Y. L.; Lang, D. V.; Rogers, J. A.; Hsu, J. W. P. *Nano Lett.* **2003**, *3*, 913−917.
(53) Duda, J. C.; Saltonstall, C. B.; Norris, P. M.; Hopkins, P. E. *J. Chem. Phys.* **2011**, *134*, 1−6.
(54) Duda, J. C.; Beechem, T. E.; Smoyer, J. L.; Norris, P. M.; Hopkins, P. E. *J. Appl. Phys.* **2010**, *108*, 073515.
(55) Lee, S.; Park, J.; Ragan, R.; Kim, S.; Lee, Z.; Lim, D. K.; Ohlberg, D. A. A.; Williams, R. S. *J. Am. Chem. Soc.* **2006**, *128*, 5745−5750.
(56) We note that the prediction by Luo and Lloyd is higher than our MD result. We believe this discrepancy to be primarily due to their use of a Morse potential to calculate the vibrational properties of the Au leads. We use an EAM potential that better reproduces the experimentally measured dispersion of Au than the Morse potential.
(57) Kogut, L.; Etsion, I. *Tribol. Trans.* **2003**, *46*, 383−390.
(58) Greenwood, J. A.; Tripp, J. H. *Proc. Inst. Mech. Eng.* **1970**, *185*, 625−633.
(59) Derjaguin, B. .; Muller, V. .; Toporov, Y. . *J. Colloid Interface Sci.* **1975**, *53*, 314−326.
(60) Muller, V. M.; Derjaguin, B. V.; Toporov, Y. P. *Colloids Surf.* **1983**, *7*, 251−259.
(61) Johnson, K. L.; Kendall, K.; Roberts, A. D. *Proc. R. Soc. London, Ser. A* **1971**, *324*, 301−313.
(62) Mahaffy, R.; Bhatia, R.; Garrison, B. J. *J. Phys. Chem. B* **1997**, *101*, 771−773.
(63) Sung, I. H.; Kim, D. E. *Appl. Phys. A: Mater. Sci. Process* **2005**, *81*, 109−114.
(64) Seong, M.; Singh, P. K.; Sinha, S. *J. Appl. Phys.* **2013**, *113*, 024321.
(65) Prasher, R. S.; Phelan, P. E. *J. Appl. Phys.* **2006**, *100*, 063538.
(66) Plimpton, S. *J. Comput. Phys.* **1995**, *117*, 1−19.
(67) Gale, J. D. *J. Chem. Soc. Faraday Trans.* **1997**, *93*, 629−637.

DOI: 10.1021/nl504844d
Nano Lett. 2015, 15, 2985−2991